Peer-reviewed version available at Entropy 2019, 21, 512; doi:10.3390/e21050512

Article

Magnetic Otto engine for an electron in a quantum dot: classical and quantum approach

Francisco J. Peña [1]*, O. Negrete[1], G. Alvarado Barrios[3,4], D. Zambrano[1], Alejandro González [1], A. S. Nunez [2], Pedro A. Orellana [1] and Patricio Vargas [1,4]

[1] Departamento de Física, Universidad Técnica Federico Santa María, Casilla 110 V, Valparaíso, Chile; oscar.negrete@usm.cl (O. N.); david.zambrano@usm.cl (D. Z.); alejandro.gonzalezi@usm.cl (A.G.); pedro.orellana.dinamarca@gmail.com (P.A.O.); patricio.vargas@usm.com (P.V.)

[2] Departamento de Física, Facultad de Ciencias Físicas y Matemáticas, Universidad de Chile, Casilla 487-3, Chile; alnunez@dfi.uchile.cl

[3] Departemento de Física, Universidad de Santiago de Chile (USACH), Avenida Ecuador 3493, 9170124, Chile; gabriel.alvarado@usach.cl

[4] Centro para el Desarrollo de la Nanociencia y la Nanotecnología, Santiago, Chile

* Correspondence: f.penarecabarren@gmail.com ; francisco.penar@usm.cl

Version January 9, 2019 submitted to

Abstract: We study the performance of a classical and quantum magnetic Otto cycle with a quantum dot as a working substance using the Fock-Darwin model with the inclusion of the Zeeman interaction. Modulating an external/perpendicular magnetic field, we found in the classical approach an oscillating behavior in the total work that is not perceptible under the quantum formulation. Also, we compare the work and efficiency of this system for different regions of the Entropy, $S(T, B)$, diagram where we found that the quantum version of this engine always shows a reduced performance in comparison to his classical counterpart.

Keywords: Magnetic cycle; Quantum Otto cycle; Quantum Thermodynamics.

1. Introduction

The study of quantum heat engines (QHEs) [1] is focused on the search and design of efficient nanoscale devices operating with a quantum working substance. These devices are characterized by their working substance, the thermodynamic cycle of operation, and the dynamics that govern the cycle [2–26]. Amongst the cycles in which the engine may operate, the Carnot and Otto cycles have received increasing attention. In particular, the quantum Otto cycle has been considered for various working substances such as, spin-1/2 systems [27,28], harmonic oscillators [29], among others. Furthermore, the quantum Otto cycle has been experimentally realized in trapped-ions [30].

Previous studies of the quantum Otto cycle embedding working substances with magnetic properties have highlighted the role of degeneracy in the energy spectrum on the performance of the engine. [31–33]. In this same framework, we highlight the work of Mehta and Ramandeep [34], who worked on a quantum Otto engine in the presence of level degeneracy, finding an enhancement of work and efficiency for two-level particles with a degeneracy in the excited state. Also, Azimi et al. presented the study of a quantum Otto engine operating with a working substance of a single phase multiferroic $LiCu_2O_2$ tunable by external electromagnetic fields [35] and is extended by Chotorlishvili et al. [36] under the implementation of shortcuts to adiabaticity, finding a reasonable output power for the proposed machine. Recently an electron confined inside a semiconductor quantum dot has been studied in the context of an isoenergetic cycle [37]. This system is externally driven by an external magnetic field finding that in the high magnetic field regime the efficiency achieves the asymptotic limit in agreement with results previously reported in the literature for mechanically driven quantum engines. On the other hand, the classical version of the Otto cycle consists of two isochoric processes and two adiabatic processes. If the working substance is a classical ideal gas, the first approximation for efficiency depends on the quotient of the temperatures in the first adiabatic compression. This

Peer-reviewed version available at Entropy 2019, 21, 512; doi:10.3390/e21050512

expression is reduced with the specific condition along the adiabatic trajectory for this kind of gas, given by $TV^{\gamma-1} = cnt.$, where $\gamma = C_P/C_V$ obtaining the expression $\eta = 1 - \frac{1}{r^{\gamma-1}}$, where r is called "compression ratio" that is defined as V_1/V_2 (with $V_1 > V_2$). For magnetic substances, like diamagnetic systems, the condition obtained for the adiabatic stroke, in general, is not trivial. This is due to the complexity of the energy spectra as a function of the external magnetic field for this kind of systems. This is later reflected in the partition function from which the thermodynamic quantities under study are obtained. In particular, it is interesting the comparison of the classical and quantum approaches for the same magnetic working substance and establish the conditions for each case appropriately. Besides, physically it is nowadays possible to confine electrons in 2D. For instance, quantum confinement can be achieved in semiconductor hererojunctions, such as GaAs and AlGaAs. At $T = 300$ K, the band gap of GaAs is 1.43 eV while it is 1.79 eV for AlxGa1-xAs (x=0.3). Thus, the electrons in GaAs are confined in a 1-D potential well of length L in the Z-direction. Therefore, electrons are trapped in 2D space, where a magnetic field along Z-axis can be applied [38].

Therefore, in this work, we study the performance of a multi-level classical and quantum Otto cycle where the working substance comprises a nanosized quantum dot under a controllable external magnetic field. This system is described by the Fock-Darwin model [39,40] that represents an accurate model for a semiconductor quantum dot.

2. Model

Let us consider an system given by a electron in the presence of a parabolic potential and external magnetic field **B**. The Hamiltonian which describes the system is given by

$$\hat{\mathcal{H}} = \frac{1}{2m^*}\left(\mathbf{p} + e\mathbf{A}\right)^2 + U_D(x,y), \tag{1}$$

where m^* is the effective electron mass, **A** is the total vector potential, and the term $U_D(x,y)$ is given by

$$U_D(x,y) = \frac{1}{2}m^*\omega_0^2\left(x^2 + y^2\right), \tag{2}$$

which corresponds to an attractive potential describing the effect of the dot on the electron. The quantity ω_0 is the parabolic trap frequency and can be controlled geometrically. If we consider a constant perpendicular magnetic field in the form

$$\mathbf{B} = B\hat{z}\,, \tag{3}$$

and the use of the vector potential **A** in the symmetric gauge (i. e. $\mathbf{A} = \frac{B}{2}(-y, x, 0)$), the solution of the eigenvalues of the Schrödinger equation are given by

$$E_{nm} = \hbar\Omega\left(2n + \mid m \mid +1\right) + \frac{1}{2}\hbar\omega_c m. \tag{4}$$

where, $\omega_c = \frac{eB}{m^*}$ is the cyclotron frequency, n, m are the radial and magnetic quantum numbers (n=0,1,2,... and m=$-\infty$,...,$+\infty$). Ω it is known as the effective frequency of the system corresponding to

$$\Omega = \omega_0\left(1 + \left(\frac{\omega_c}{2\omega_0}\right)^2\right)^{\frac{1}{2}}. \tag{5}$$

Notice that when the parameter $\omega_0 \to 0$, the energy levels of Equation (4), take the usual form of the Landau energy levels in cylindrical coordinates.

Preprints (www.preprints.org) | NOT PEER-REVIEWED | Posted: 9 January 2019 doi:10.20944/preprints201901.0079.v1

Peer-reviewed version available at Entropy 2019, 21, 512; doi:10.3390/e21050512

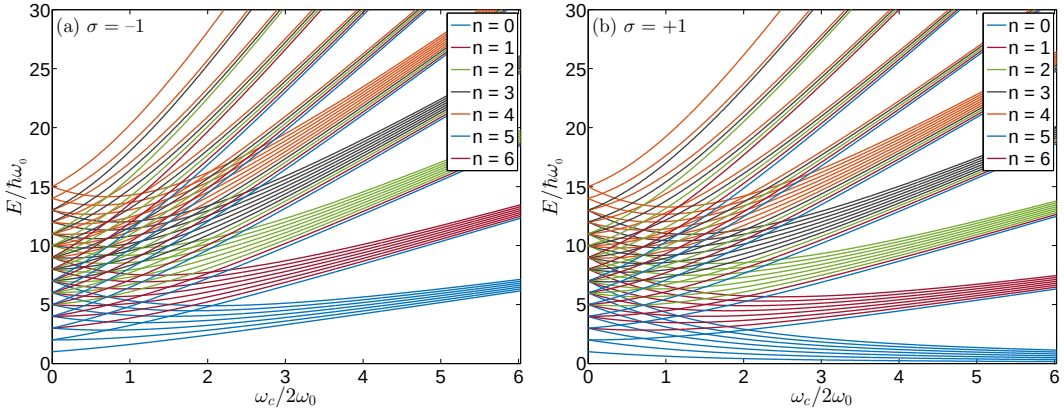

Figure 1. (a) Fock-Darwin energy spectrum with $s = +1$ for the first six radial number $n = 0, 1, ..., 6$ and for each of them the azimuthal quantum number taking the values between $m = -6, -5, ..., 5, 6$. (b) Fock-Darwin energy spectrum with $s = -1$ for the first six radial number $n = 0, 1, ..., 6$ and for each of them the azimuthal quantum number taking the values between $m = -6, -5, ..., 5, 6$. We clearly observe the confinement of the energy levels at high magnetic fields $(\omega_c/2\omega_0 >> 1)$.

To obtain a more precise calculation, especially when we consider the case of strong magnetic fields for the electron trapped in a quantum dot, we also take into account the electron spin of value $\frac{\hbar\hat{\sigma}}{2}$ and magnetic moment μ_B, where $\hat{\sigma}$ is the Pauli spin operator and $\mu_B = \frac{e\hbar}{2m^*}$. Here the spin can have two possible orientations, one is $\uparrow$ or $\downarrow$ with respect to the applied external magnetic field B in the direction of the z-axis. Therefore, we need to add the Zeeman term in the Fock-Darwin energy levels Equation (4). Consequently, the new energy spectrum is given by

$$E_{n,m,\sigma} = \hbar\Omega(2n + |m| + 1) + m\frac{\hbar\omega_c}{2} - \mu_B\sigma B. \tag{6}$$

The energy spectrum of Equation (6) is presented in Figure (1) for $\sigma = -1$ and $\sigma = 1$. It is interesting to note that for high magnetic fields $(\omega_c/2\omega_0 >> 1)$ things simplify in Eq. (6) and we get the following expression:

$$E_{n,m,\sigma} = \frac{\hbar\omega_c}{2}(n + 1/2 + |m| + m) - \mu_B\sigma B\ , \tag{7}$$

where we observe that $|m| + m = 0$ for $m < 0$, therefore each Landau level labelled by n has infinite degeneracy.

In our calculations along the work, we will consider a low-frequency coupling for the parabolic trap given by $\omega_0 \sim 0.2637\ THz$ which in terms of energy units corresponds to a coupling of approximately $1.5\ meV$. The selection of this particular value is to compare the intensity of the trap with the typical energy of intra-band optical transitions of the quantum dots [39]. The order of this transition is approximately around $\sim 1\ meV$ for cylindrical GaAs quantum dots with effective mass given by $m^* \sim 0.067\ m_e$ [39,40].

Throughout the discussion of this work, for the classical approach, we use the Refs. [41,42,44,45] and in particular, classical thermodynamics quantities for the Fock Darwin model with spin can be obtained analytically using the treatment of Kumar *et. al.* [46] using the partition function, which can be written as:

$$\mathcal{Z}_{dS} = \frac{1}{2}\mathrm{csch}\left(\frac{\hbar\beta\omega_+}{2}\right)\mathrm{csch}\left(\frac{\hbar\beta\omega_-}{2}\right)\cosh\left(\frac{\hbar\beta\omega_B}{2}\right). \tag{8}$$

where the frequencies $\omega_\pm$ are:

Preprints (www.preprints.org) | NOT PEER-REVIEWED | Posted: 9 January 2019 doi:10.20944/preprints201901.0079.v1

Peer-reviewed version available at Entropy 2019, 21, 512; doi:10.3390/e21050512

$$\omega_{\pm} = \Omega \pm \frac{\omega_c}{2}. \tag{9}$$

Therefore, entropy $(S(T,B))$, internal energy $(U(T,B))$ and magnetization $M(T,B)$ are simply given by

$$S(T,B) = k_B \ln \mathcal{Z}_{dS} + k_B T \left(\frac{\partial \ln \mathcal{Z}_{dS}}{\partial T} \right)_B, \tag{10}$$

$$U(T,B) = k_B T^2 \left(\frac{\partial \ln \mathcal{Z}_{dS}}{\partial T} \right)_B, \tag{11}$$

$$M(T,B) = k_B T \left(\frac{\partial \ln \mathcal{Z}_{dS}}{\partial B} \right). \tag{12}$$

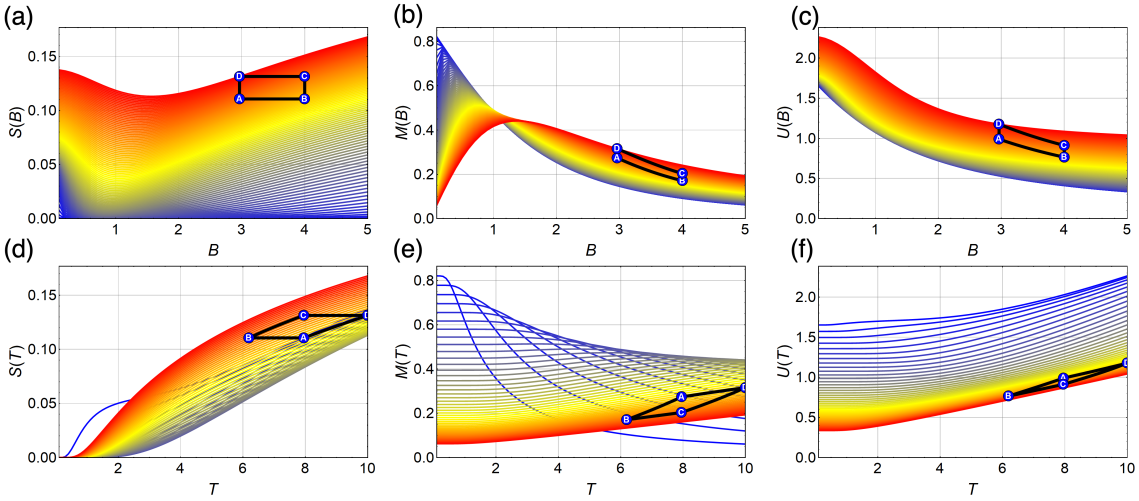

Figure 2. Classical thermodynamics quantities entropy (S), internal energy (U) and magnetization (M) as a function of temperature (T) (panels (a) to (c)) and external magnetic field (B) (panels (d) to (f)). For (a) to (c) panels the color blue to red represent temperatures from 0.1 K to 10 K respectively . For (d) to (f) panels the colors blue to red represent lower to higher external magnetic field, from 0.1 T to 5 T. The value of the parabolic trap correspond approximately to 1.5 meV. Additionally, we plot the proposal cycle on each of the aforementioned thermodynamic quantities.

The Equations (10), (11) and (12) are presented in the Figure 2 for a parabolic trap corresponding to an energy of 1.5 meV together with the scheme of the proposed cycle. A very interesting behaviour is observed for the entropy as a function of the magnetic field in the panel (a) of Figure 2. For external magnetic fields $\leq$ 1 T, the entropy shows a decreasing behaviour as the external field increase, but for values higher than 1 T contrary behaviour is found. This can be explained due to strong degeneracy of the energy levels for higher magnetic fields. This degeneracy in the energy levels explains the entropy growth together with the external magnetic field applied to the sample. Also, the change in the behaviour of the entropy is affected by temperature, finding that the change of slope as a function of external magnetic field moves away from the 1 T value to higher values in as we increase the temperature of the working substance. This can be appreciated in the (a) panel of Figure (2). At the same time, the magnetization shows a crossing in its behaviour as a function of magnetic field as we can see in the (b) panel of Figure (2), where previous to this crossing at lower temperatures higher values of magnetization are obtained. This fact will become essential for the total work extracted. In the cycle that we propose, the work is directly related to the change in the magnetization of the system as a function of magnetic field and temperature. On the other hand, we can observe that the internal energy does not present qualitative changes and shows a decreasing of its value as the field

Preprints (www.preprints.org) | NOT PEER-REVIEWED | Posted: 9 January 2019 doi:10.20944/preprints201901.0079.v1

Peer-reviewed version available at Entropy 2019, 21, 512; doi:10.3390/e21050512

increases for all temperatures displayed. The reason for this is that the internal energy only depends on the derivative of $\ln \mathcal{Z}_{dS}$ (see Equation (11)) with respect to temperature while the entropy has an additional term proportional to $\ln \mathcal{Z}_{dS}$ (see Equation (10)) and the magnetization on its derivative with respect to the external field (see Equation (12)).

It is important to mention that the cycle operation in the counter-clockwise form starting in the A point described in Figure 2 gives negative work extracted, so to define a thermal machine correctly, we start the cycle in the point B, and we go through it in a clockwise direction. This is due to the particular behaviour of the entropy as a function of magnetic field and temperature in the chosen zone marked with A, B, C and D. Therefore, the cycle that will describe in the next subsection is the form of B $\rightarrow$ A $\rightarrow$ D $\rightarrow$ C $\rightarrow$ B and is presented in ~~the~~ Figure 3.

3. First Law of Thermodynamics and the Quantum and Classical Otto Cycle

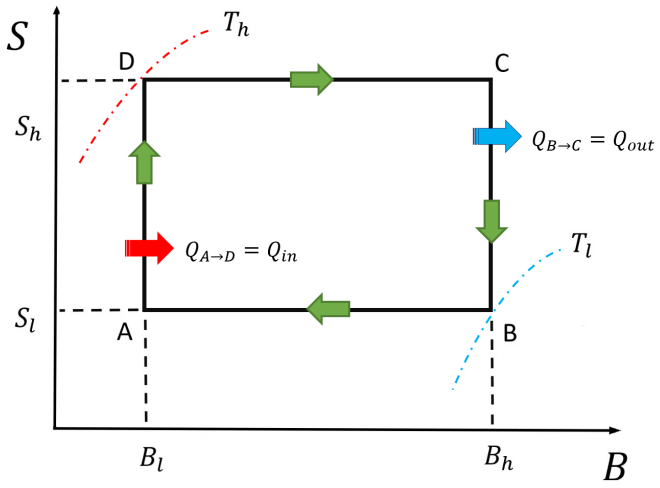

Figure 3. The magnetic Otto engine represented as an entropy (S) versus a magnetic field (B) diagram. The way to perform the cycle is in the form B $\rightarrow$ A $\rightarrow$ D $\rightarrow$ C $\rightarrow$ B.

The first law of thermodynamics in a quantum context has been discussed extensively in the literature. We will follow the treatment of Refs. [41,42,44], which identifies the heat transferred and work performed during a thermodynamic process by means of the variation of the internal energy of the system.

First, consider a system described by a Hamiltonian, $\hat{\mathcal{H}}$, with discrete energy levels, $E_{n,m,\sigma}$. The internal energy of the system is simply the expectation value of the Hamiltonian $E = \langle \hat{\mathcal{H}} \rangle = \sum_n \sum_m \sum_\sigma p_{n,m,\sigma} E_{n,m,\sigma}$, where $p_{n,m,\sigma}$ are the corresponding occupation probabilities. The infinitesimal change of the internal energy can be written as

$$dE = \sum_n \sum_m \sum_\sigma \left(E_{n,m,\sigma} dP_{n,m,\sigma} + P_{n,m,\sigma} dE_{n,m,\sigma} \right), \tag{13}$$

where we can identify the infinitesimal work and heat as

$$dQ := \sum_n \sum_m \sum_\sigma E_{n,m,\sigma} dp_{n,m,\sigma} \quad , \qquad dW := \sum_n \sum_m \sum_\sigma p_{n,m,\sigma} dE_{n,m,\sigma}. \tag{14}$$

Equation (13) is the formulation of the first law of thermodynamics for quantum working substances. Therefore, work is then related to a change in the eigenenergies $E_{n,m,\sigma}$, which is in agreement with the fact that work can only be carried out through a change in generalized coordinates.

The quantum Otto cycle is composed by four strokes: two quantum isochoric processes and two quantum adiabatic processes. This cycle can be seen in Figure 3 replacing the value of S_l and S_h for $P_{n,m,\sigma}(T_l, B_h)$ and $P_{n,m,\sigma}(T_h, B_l)$ in the vertical axe respectively. For the cases that we will consider, the quantum Otto cycle proceeds as follows.

1. Step B $\rightarrow$ A: Quantum adiabatic compression process. The systems is isolated from the cold reservoir and the magnetic field is changed from B_h to B_l, with $B_h > B_l$. During this stage the populations remain constant, so $P_{n,m,\sigma}(T_l, B_h) = P^{\mathrm{A}}_{n,m,\sigma}$. We recall that $P^{\mathrm{A}}_{n,m,\sigma}$ is not a thermal state. No heat is exchanged during this process.

2. Step A $\rightarrow$ D: The systems, at constant magnetic field B_l, is brought into contact with a hot thermal reservoir at temperature T_h until it reaches thermal equilibrium. The corresponding thermal populations $P_{n,m,\sigma}(T_h, B_l)$ are given by the Boltzmann distribution with temperature T_h. No work is done during this stage.

The heat absorbed for the working substance is given by

$$Q_{in} = \sum_n \sum_m \sum_\sigma \int_{\mathrm{A}}^{\mathrm{D}} E_{n,m,\sigma} dP_{n,m,\sigma} = \sum_n \sum_m \sum_\sigma E^l_{n,m,\sigma} \left[P_{n,m,\sigma}(T_h, B_l) - P^{\mathrm{A}}_{n,m,\sigma} \right], \tag{15}$$

where $E^l_{n,m,\sigma}$ is the nth eigenenergy of the system in the quantum isochoric heating process to an external magnetic field of value B_l .

3. Step D $\rightarrow$ C: Quantum adiabatic expansion process. The system is isolated from the hot reservoir, and the intensity of magnetic field is changed back from B_l to B_h. During this stage the populations remains constant, so $P_{n,m,\sigma}(T_h, B_l) = P^{\mathrm{C}}_{n,m,\sigma}$. Again, we recall that $P^{\mathrm{C}}_{n,m,\sigma}$ is not a thermal state. No heat is exchanged during this process.

4. Step C $\rightarrow$ B : Quantum isochoric cooling process. The working substance at B_h is brought into contact with a cold thermal reservoir at temperature T_l. Therefore, the heat released is given by

$$Q_{out} = \sum_n \sum_m \sum_\sigma \int_{\mathrm{C}}^{\mathrm{B}} E_{n,m,\sigma} dP_{n,m,\sigma} = \sum_n \sum_m \sum_\sigma E^h_{n,m,\sigma} \left[P_{n,m,\sigma}(T_l, B_h) - P^{\mathrm{C}}_{n,m,\sigma} \right], \tag{16}$$

where $E^h_{n,m,\sigma}$ is the nth eigenenergy of the system in the quantum isochoric heating process to an external magnetic field of value B_h.

The net work done in a single cycle can be obtained from $W = Q_{in} + Q_{out}$,

$$W = \sum_n \sum_m \sum_\sigma \left(E^l_{n,m,\sigma} - E^h_{n,m,\sigma} \right) \left(P_{n,m,\sigma}(T_h, B_l) - P_{n,m,\sigma}(T_l, B_h) \right), \tag{17}$$

where we have used the condition of constant populations along the quantum adiabatic strokes. Furthermore, the efficiency is given by

$$\eta = \frac{W}{Q_{in}}. \tag{18}$$

The main differences between the classical and quantum Otto cycle is related to the point A and D in the cycle. In classical engine, the works presented in Equation (15) and Equation (16), can be calculated replacing $P^A_{n,m,\sigma}$ by $P(T_A, B_l)$ and $P^C_{n,m,\sigma}$ by $P(T_C, B_h)$ obtaining a difference between the classical internal energy derived from the partition function in the form

$$Q_{in} = U(T_h, B_l) - U(T_A, B_l); \qquad Q_{out} = U(T_l, B_h) - U(T_C, B_h), \tag{19}$$

where T_{A} and T_{C} they are determined by the condition imposed by the classical isentropic strokes. If we have the classical entropy, the intermediate temperatures T_{A} and T_{C} can be determined in two different forms:

Peer-reviewed version available at Entropy 2019, 21, 512; doi:10.3390/e21050512

- Finding the relation between the magnetic field and the temperature along an isentropic trajectory by solving the differential equation of first order given by

$$dS(B,T) = \left(\frac{\partial S}{\partial B}\right)_T dB + \left(\frac{\partial S}{\partial T}\right)_B dT = 0, \tag{20}$$

which can be written as

$$\frac{dB}{dT} = -\frac{C_B}{T\left(\frac{\partial S}{\partial B}\right)_T}, \tag{21}$$

where C_B is the specific heat at constant magnetic field.

- The other possibility is to connect the entropy values of two isentropic trajectories in the form

$$\begin{aligned} S(T_l, B_h) &= S(T_{\mathrm{A}}, B_l) \\ S(T_h, B_l) &= S(T_{\mathrm{C}}, B_h)\,, \end{aligned} \tag{22}$$

finding the magnetic field in terms of the temperature, throughout numerical calculation.

Therefore, from the Equation (19) and $W = Q_{in} + Q_{out}$, the classical work is given by the difference of four internal energy in the form

$$W = U_{\mathrm{D}}\left(T_h, B_l\right) - U_{\mathrm{A}}\left(T_{\mathrm{A}}, B_l\right) + U_{\mathrm{B}}\left(T_l, B_h\right) - U_{\mathrm{C}}\left(T_C, B_h\right), \tag{23}$$

In the following section, the units of temperature correspond to Kelvin (K), and the external field is in units of Tesla (T). The thermodynamics quantities entropy (S), magnetization (M) and internal energy (U), are in units of $\frac{meV}{\mathrm{K}}$, $\frac{meV}{T}$ and meV respectively. The total work extracted is in the units of meV. The maximum values considered in our calculations for the temperatures and external magnetic field are 10 K and 5 T. Therefore, for the quantum cycle calculation (i. e. Equation (17)), we use the quantum numbers $n = 0$ to $n = 10$ and $m = -33$ to $m = 33$ of Equation (6). The selection of this particular energy levels in this model is justified for the values of the thermal populations for the hot and cold temperatures of the reservoirs that we have selected. Our numerical calculations indicated that the contributions of the other levels of energy can be neglected.

Finally, it is useful to express our results of total work extracted and efficiency in terms of the relation between the highest value (B_h) and the lowest value (B_l) of the external magnetic field over the sample. To do that, we use the definition of "magnetic length" which is given by

$$l_B = \sqrt{\frac{\hbar}{eB}}, \tag{24}$$

allowing us to define the parameter

$$r = \frac{l_{B_l}}{l_{B_h}} = \sqrt{\frac{B_h}{B_l}}, \tag{25}$$

which represents the analogy of the compression ratio for the classical case. It is important to remember that the Landau radius is inversely proportional to the magnitude of the magnetic field. Therefore, for a major (minor) magnitude of the field, the Landau radius is smaller (bigger), and the r is well defined.

Preprints (www.preprints.org) | NOT PEER-REVIEWED | Posted: 9 January 2019 doi:10.20944/preprints201901.0079.v1

Peer-reviewed version available at Entropy 2019, 21, 512; doi:10.3390/e21050512

4. Results and Discussions

4.1. Classical Magnetic Otto Cycle

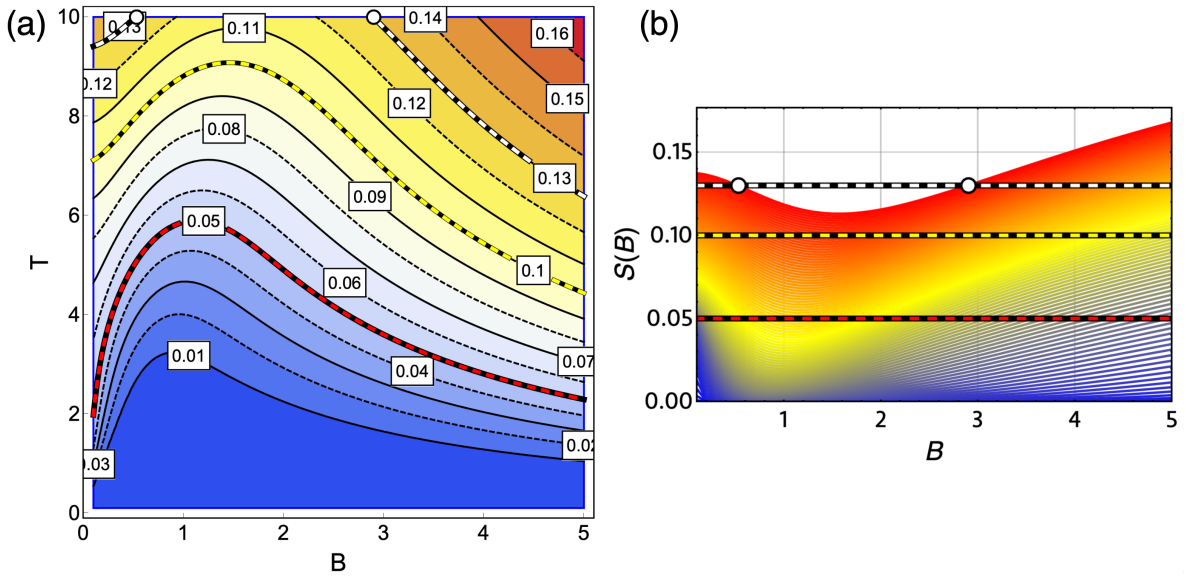

Figure 4. Solution of classical isentropic path. The panel (a) shows the entropy as a function of magnetic field (horizontal axis) and temperature (vertical axis). The level curves (constant entropy values) highlights three different values for low (red-black curve, $S = 0.05$), middle (yellow-black curve, $S = 0.10$) and high (white-black curve, $S = 0.13$). The (b) panel shows the three constant values for the entropy ($S = 0.05, S = 0.10, S = 0.13$) in a graphic of entropy as a function of B for temperatures from 1 K (blue) up to 10 K (red). Due to the form of the entropy obtained for this system, the solution for $S = 0.13$ needs to work with temperatures higher than 10 K for an external magnetic field lower than 3 T (white dots in the (a) and (b) panel of this figure). The value of the parabolic trap corresponds to 1.5 *meV*

The condition gives by Equation (21) (or Equation (22)) for the classical cycle give us the information about the behaviour of the external magnetic field and the temperature in the adiabatic stroke. In the (a) panel of Figure 4, we can appreciate the level curves of the entropy function $S(T, B)$ and in the (b) panel some examples of isentropic strokes in a plot of $S(B)$ vs B for different temperatures. That example shows three cases of constant entropy for a low (red-black curve, $S = 0.05$), middle (yellow-black curve, $S = 0.10$) and high (white-black curve, $S = 0.13$). We observe in the (a) panel of Figure (4) that there is a zone where the external field grows with the temperature of the sample and a zone where the opposite happens in order to maintain the entropy constant. At low working temperatures, the behaviour changes near $B = 1$ T, while as the temperature increases, the slope change occurs at higher values of the magnetic field, approaching $B = 2$ T. Secondly, if we observe the (b) panel of Figure (4) the case for $S = 0.13$ (white-black line), we have a restricted area for field values lower to 3 T if we work with a maximum temperature of 10 K. Therefore, it is not arbitrary the movement of the magnetic field if we think in a thermodynamic magnetic Otto cycle with two temperature reservoirs fixed at some specific values, more specifically, the reservoir associated to the hot temperature in the cycle. Also, the Figure 4 is the solution of $S(T, B) =$ constant, obtained from the differential Equation (21) with different conditions (i. e. distinct values of the constant value of S). Therefore, panel (a) of Figure 4 depicts all family of solutions for the isentropic stroke of the engine of this particular system.

Preprints (www.preprints.org) | NOT PEER-REVIEWED | Posted: 9 January 2019 doi:10.20944/preprints201901.0079.v1

Peer-reviewed version available at Entropy 2019, 21, 512; doi:10.3390/e21050512

In our first example displayed in the Figure (5), the B point has the value of the external field given by $B_{\rm h} = 4$ T and a temperature of $T_{\rm B} = 6.19$ K. The value of the temperature for the D point is fixed to $T_{\rm D} = 10$ K. Therefore, the Carnot efficiency of the proposal cycle is given by

$$\eta_{Carnot} = 1 - \frac{T_{\rm B}}{T_{\rm D}} = 1 - \frac{6.19}{10} = 0.381 \tag{26}$$

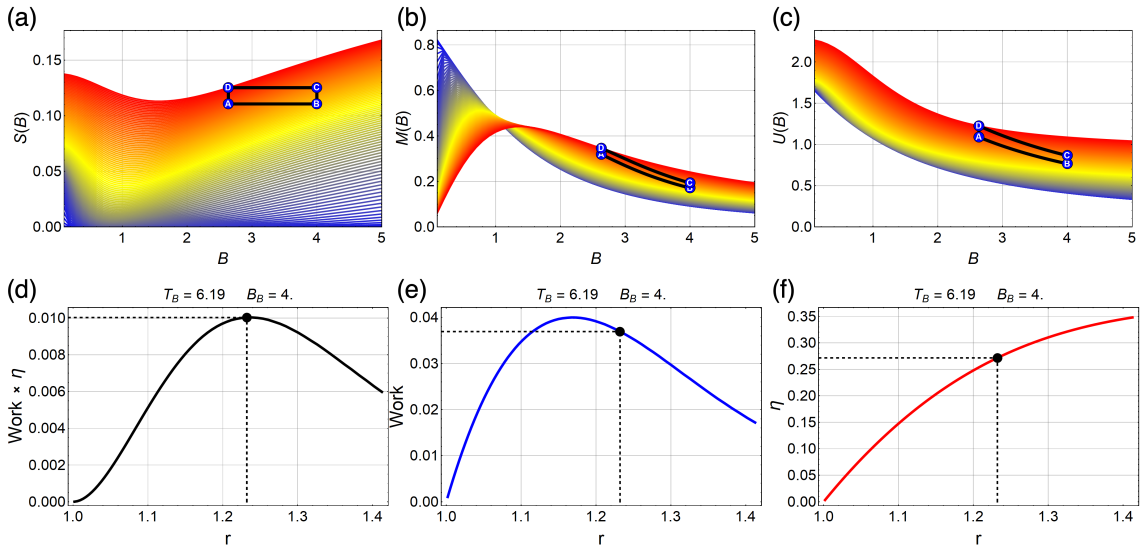

Figure 5. Proposed magnetic Otto cycle showing three different thermodynamics quantities, Entropy (S), Magnetization (M) and Internal Energy (U) ((a) to (c) panel respectively) as a function of the external magnetic field and different temperatures from $0.1K$ (blue) to $10K$ (red). Panel (d) shows the total work extracted multiplied by efficiency $(W\eta)$, (e) shows the total work extracted (W) and (f) the efficiency (η) for the classical cycle. The black points in the panels (d) to (f) represent exactly the cycle B $\rightarrow$ A $\rightarrow$ D $\rightarrow$ C $\rightarrow$ B, presented in the panels (a) to (c). The value of the parabolic trap corresponds to 1.5 meV. The fixed temperatures are $T_{\rm B} = 6.19$ K and $T_{\rm D} = 10$ K.

The low central panel (e) of the Figure 5 shows different values of total work extracted (W) varying the value of $B_{\rm D}$ from 4 T to 1.99 T. This variation in the external field is reflected in the movement of r in the form of $r = \sqrt{\frac{4}{B_{\rm l}}}$. Therefore, r is in the range of $1 \leq r \leq 1.41$. The parabolic trap is fixed to the value of 1.5 meV and the effective mass in the value of $m^* = 0.067m_e$. In particular, the (a) to (c) panels of the Figure 5 shows the exact paths for the magnetic cycle for the maximum point obtained when multiplying W ((e) panel) and the efficiency (η, (f) panel). That point corresponds to $r \sim 1.22$ (black point in the (d) to (f) panels of the Figure 5 and constitutes the best configuration of the systems in order to obtain the best W with the better η through the cycle. Also, W and η are presented in (e) and (f) panel of Figure 5 for the optimal value of r parameter mentioned before. We observe that W obtained for that point is in the order of ~ 0.038 meV with an efficiency of $\eta \sim 0.28$. We verified the numeric value of total work extracted using the area enclosed by the cycle in the graph of M versus B of Figure 5 panel (b) due to the fact that the work is $W = -\int MdB$ [37,42,44] when the parameter changed during the operation of the engine is the external field. On the other hand, to obtain the solid lines presented in the (d) to (f) panels in Figure 5 we need to make different cycles configuration keeping the values of the isothermal fixed as can be appreciated in the *Supplemental Material I*, made with the Mathematica software [43], where we show each shape that the cycle must have to generate a point of work in specific. It is important to recall that we never reach the optimal value of $\eta = 0.381$, i.e. the Carnot efficiency.

Due to the change of behaviour in the entropy as a function of the external field, we obtain a very interesting results for W when we explore the zone close and around to $B = 1$ T. Before that

point, the entropy decrease as function of the external field (B) and after that point entropy begins to increase. This fact can be used to explore the magnetic cycle in that zone finding an oscillatory behaviour for W. In the Figure 6 we show the cycle with operating temperatures $T_{\mathrm{B}} = 2.69$ K and $T_{\mathrm{D}} = 5.40$ K and external magnetic field moving between 2.995 T to 0.250 T and consequently, the r parameter move from 1 to 3.46. First, we observe a decreasing efficiency for $r > 1.75$ in the (f) panel of Figure 6 with a maximum value of $\eta \sim 0.43$ for $r \sim 1.75$. Therefore, for this configuration, the Carnot efficiency ($\eta_{Carnot} \sim 0.5$ for this case) also can not be reached. In order to compare this results with the previously discussed (when we avoid this particular region) we can see from the (f) panel of Figure 5 that the efficiency asymptotically approaches to the efficiency of Carnot if we increase the intensity of the external magnetic field of the starting point of the cycle (point B).

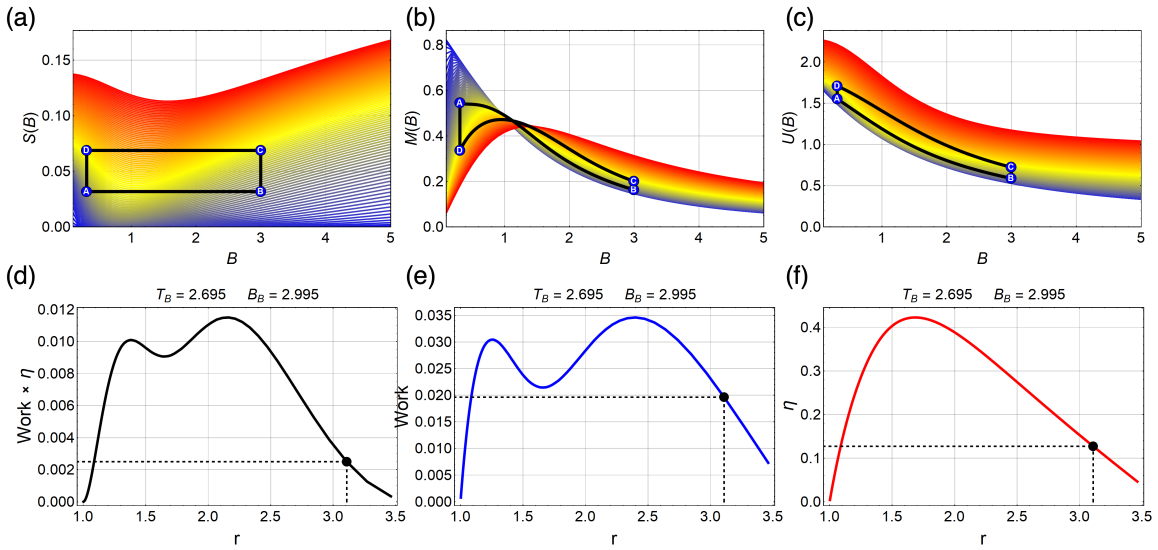

Figure 6. Proposed magnetic Otto cycle in three different thermodynamics quantities, Entropy, Magnetization and internal energy ((a) to (c) panels respectively) as a function of the external magnetic field and different temperatures from $0.1K$ (blue) to $10\ K$ (red). Total work extracted multiplied by efficiency $(W\eta)$ (d) total work extracted (W) (e) and efficiency (η) (d) for the cycle. The black point in the panels (d) to (f) represent the value of $0.02\ meV$ of total work extracted and corresponds exactly to the cycle B $\rightarrow$ A $\rightarrow$ D $\rightarrow$ C $\rightarrow$ B, showed in the panels (a) to (c). The value of the parabolic trap correspond to $1.5\ meV$. The fixed temperatures are $T_{\mathrm{B}} = 2.69$ K and $T_{\mathrm{D}} = 5.40$ K.

From panel (b) of Figure 6, we can understand the oscillations in W interpreting these results using the expression $W = -\int MdB$. Observing the (a) to (c) panels of Figure 6, the presented A,B,C,D points correspond to the black point displayed in the (d) to (f) panels where we see that the work is still greater than zero but close to a vanishing situation. The reason why there is still positive work in this point under study, is that the total area enclosed to the right of the crossing point is larger than the other in the left. The magnetization presented in the (b) panel of Figure 6 in the zone around the range of external magnetic field explored for this case (from 2.995 to $0.250T$) clearly reverses his behaviour and presents a crossing point close to $B \sim 1.2$ T for different temperatures. The area to the right of that point can be interpreted as a positive contribution to W while the left area contributes to negative work.

Preprints (www.preprints.org) | NOT PEER-REVIEWED | Posted: 9 January 2019 doi:10.20944/preprints201901.0079.v1

Peer-reviewed version available at Entropy 2019, 21, 512; doi:10.3390/e21050512

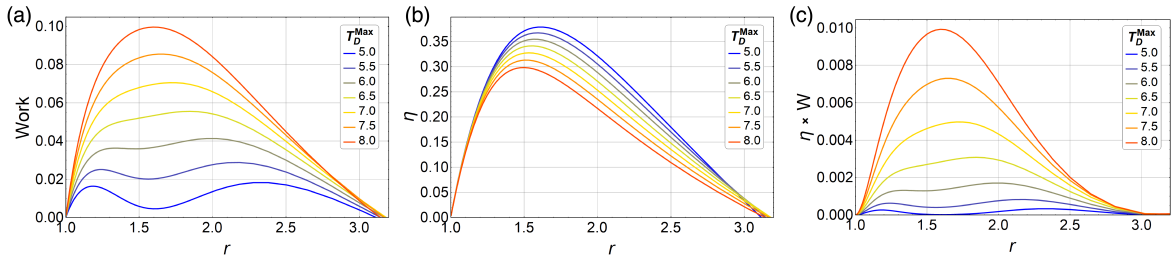

Figure 7. Work, efficiency and work multiply by efficiency ((a) to (c) panels) for different values of T_{D} for $T_{\mathrm{B}} = 2.69$ fixed. The value of the parabolic trap corresponds to 1.5 meV.

To explore if these oscillations in W are still obtained for higher temperature ranges, we plot in Figure 7 the work W for different values of T_{D} with $T_{\mathrm{B}} = 2.69$ K fixed. We note that for higher temperatures than 7 K the oscillations found before disappear. It is only a reinforcement that the quantum effects of the working substance are only significant at low temperatures. On the other hand, as we expect, W grows as the difference between the temperature reservoir is larger as we can see from the (a) panel of Figure 7. However, for this case, the efficiency obtained is increasingly lower for increasingly larger temperature differences as we can appreciate from the panel (b) of Figure 7.

4.2. Magnetic Quantum Otto Cycle

Next we show the results of the evaluation of the quantum version of this magnetic Otto cycle for the same cases shown in Figure 5 and Figure 6. In the (a) panel of Figure 8, we plot the classical work (blue line) and the quantum work (red line) for the same sets of parameters of Figure 5. First, we note that the classical and quantum work are equal up to the value of $r \sim 1.07$. That means for close values of the starting external magnetic field to the B point we do not notice a difference between the classic and quantum formulation of the Otto cycle. Also, in (a) panel Figure 8, we found that we have a transition from positive work to negative work not reflected in the classic scenario close to $r \sim 1.36$.

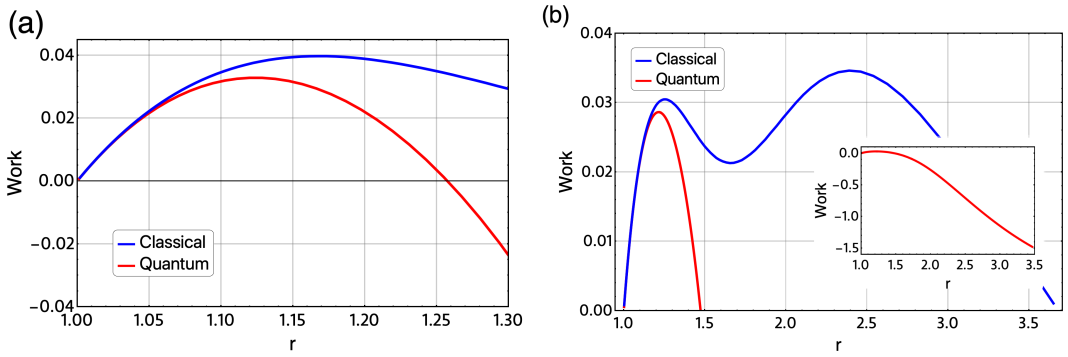

Figure 8. (a) Total work extracted for classical (blue line) and quantum version of Otto cycle (red line). The parameters for this case displayed are : $T_{\mathrm{D}} = 10$ K, $T_{\mathrm{B}} = 6.19$ K and $B_{\mathrm{B}} = 4$ T as starting value of the external magnetic field. The value of B_{D} moves from 4 T to 1.99 T and this variation is reflected in the movement of r in the form of $r = \sqrt{\frac{4}{B_{\mathrm{D}}}}$, same parameter as the results shown in Figure 5. (b) Total work extracted (W) presented in the (e) panel of Figure 6 versus the values obtaining in the quantum version of the Otto cycle. The parameters for this figure are $T_{\mathrm{D}} = 5.40$ K, $T_{\mathrm{B}} = 2.69$ K and $B_{\mathrm{B}} = 2.995$ T and B_{D} moves from 2.995 to 0.250 T. The parabolic trap is fixed to the value of 1.5 meV and the effective mass value of $m^* = 0.067m_e$.

Additionally, we observe that the maximum positive value of the total work extracted for the quantum version of Otto cycle is reduced by approximately 0.01 meV compared to the classical counterpart. In particular, for the quantum version of this cycle, we do not found the oscillations in W

Preprints (www.preprints.org) | NOT PEER-REVIEWED | Posted: 9 January 2019 doi:10.20944/preprints201901.0079.v1

Peer-reviewed version available at Entropy 2019, 21, 512; doi:10.3390/e21050512

presented in the (e) panel of Figure 6. Moreover, we found a transition from positive to negative work at some value of the r parameter. This is dramatically reflected in the (b) panel of Figure 8, where the absolute value of W is highly increased as compared with the classical approach.

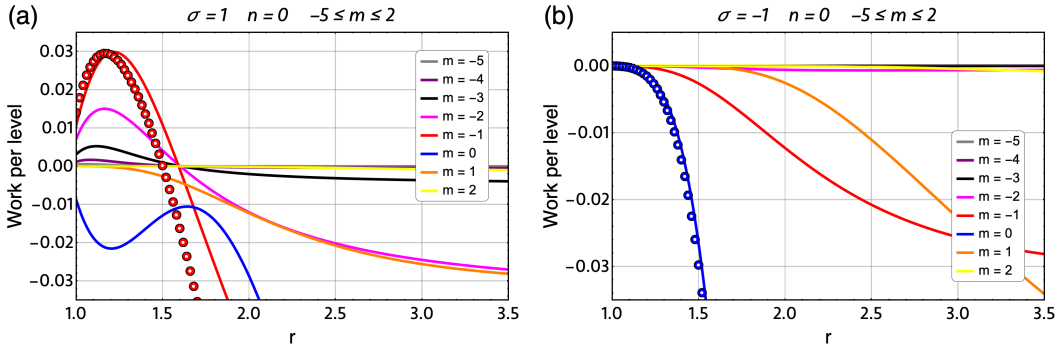

Figure 9. Total quantum work extracted (W) per energy level for the case of $\sigma = 1$ ((a) panel) and for the case of $\sigma = -1$ ((b) panel). The line marked (in the two panels) with circles correspond to the sum of all contributions of the energy level for each spin. The parameters used for this figure are the same as the one used in panel (b) of Figure(8).

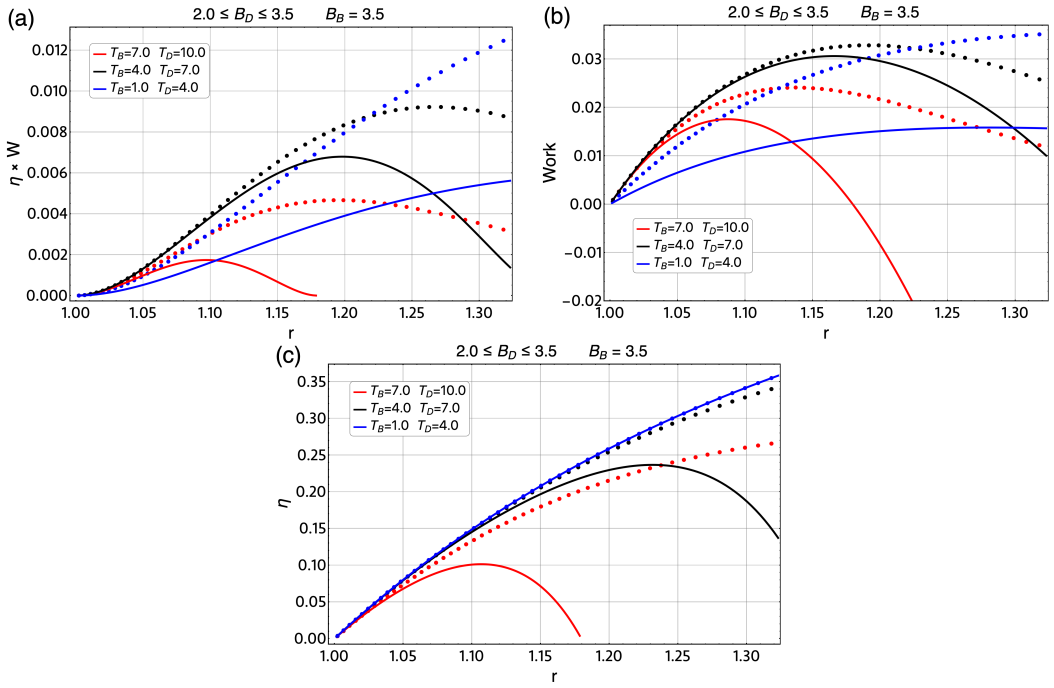

Figure 10. $\eta \times W$ (a), total work extracted (b) and (c) efficiency for the case of $\Delta T = T_h - T_l = 3\ K$ for different regions of temperature parameter for classical approach (solid line) and quantum version of the magnetic Otto cycle (dotted line). For all graphics, we use the initial external magnetic field in the value of $B_{\mathrm{B}} = 3.5$ T and the minimum value of the field, B_D moves between 3.5 T to 2.0 T. Therefore, the r parameter moves between $1 \leq r \leq 1.32$. The parabolic trap is fixed to the value of 1.5 meV and the effective mass value of $m^* = 0.067 m_e$.

In Figure 9, we present the work W per energy level and spin value for the most important values of our numerical calculations. We use the same parameter as in panel (b) of Figure 8. We observe that the contribution given by $\sigma = 1$ are positive up to r close to $r \sim 1.6$ being the energy levels $E_{0,-1}$, $E_{0,-2}$ and $E_{0,-3}$ those that contribute with the most positive values. Contrary, for the case of $\sigma = -1$ we

found that all contributions per energy level are negative. Therefore, the small region of positive work found in panel (b) of Figure 8 can be only associated to the spin up ($\sigma = 1$) contributions.

To explore other operation regions for the magnetic Otto cycle, we calculate the total work extracted and efficiency for the same $\Delta T = T_h - T_l$ in a broad range of temperatures and the same $\Delta B_{max} = 1.5$ T in different regions of the external magnetic field for the classical cycle and its quantum version. This is displayed in Figure 10 and Figure 11 where the dotted lines represent the classical results and the solid lines the quantum results. The three regions of temperature selected for this two figures are between 1 K to 4 K (blue lines), 4 K to 7 K (black lines) and 7 K to 10 K (red lines). First, we treat the case of $B_{\mathrm{B}} = 3.5$ T and B_{D} moving from 3.5 T to 2.0 T in the Figure 10, where we note large differences between the classical and quantum results for W as can be seen in the (b) panel of that figure. On the other hand, if we observe the region of $3.5 \leq B_{\mathrm{D}} \leq 5.0$ T for a B_{B} fixed shown in the (b) panel of Figure 11, the work and efficiency for the region of 1 K to 4 K and 4 K to 7 K presents similar behaviour for the classical and quantum version. Only the case of 7 K to 10 K shows a larger difference between this two approaches. For the case of the efficiency, we note in the (c) panel of Figure 10 a major difference between the classical results and quantum results compare with the presented in (c) panel of Figure 11 and this is consistent with the reported results for the work W.

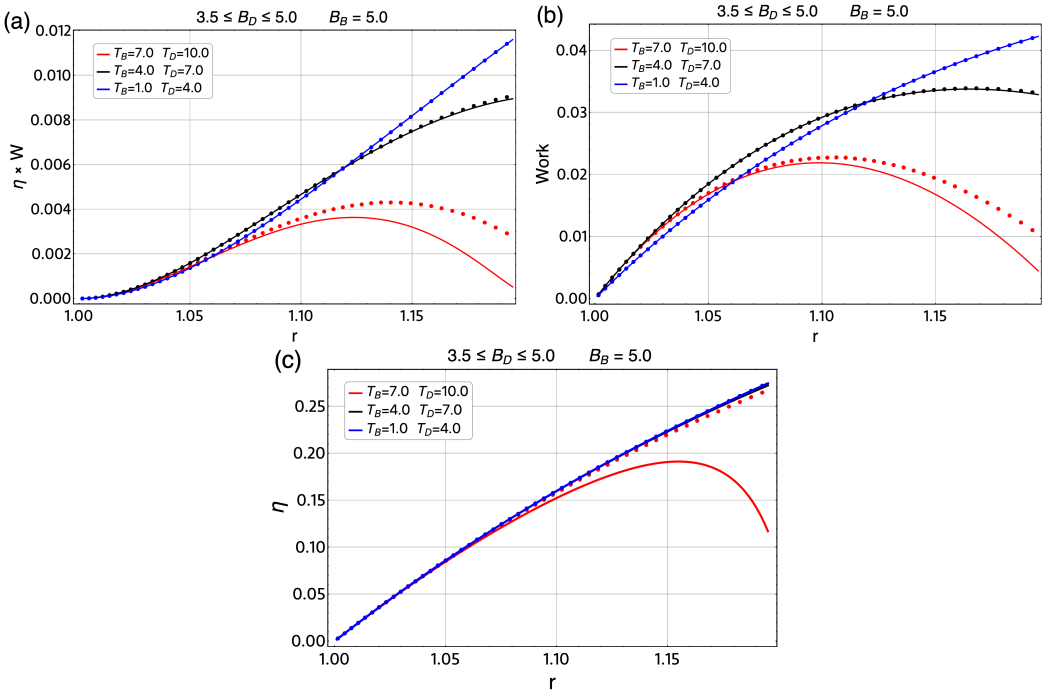

Figure 11. $\eta \times W$ (a), total work extracted (b) and (c) efficiency for the case of $\Delta T = T_h - T_l = 3\ K$ for different regions of temperature parameter. For all cases, we use the initial external magnetic field at the value of $B_{\mathrm{B}} = 5.0$ T and the minimum value of the field, B_D moves between 5.0 T to 3.5 T. Therefore, the r parameter moves between $1 \leq r \leq 1.19$. The parabolic trap is fixed to the value of 1.5 meV and the effective mass value of $m^* = 0.067 m_e$.

5. Conclusions

In this work, we explored the classical and quantum magnetic Otto cycle for an ensemble of non-interacting electrons with intrinsic spin where each one is trapped inside a semiconductor quantum dot modeled by a parabolic potential. We analyzed all relevant thermodynamics quantities, we found in particular for the entropy as a function of the external magnetic field, a zone where it diminishes as the field increases but then it increases again at larger fields, at all temperatures. This is a consequence of the infinite degeneracy that the system has at high magnetic fields, thus increasing its entropy value. This particular behavior makes the operation of the Otto engine be different depending

on the work area in temperatures and magnetic fields. We find oscillations in the total work extracted near the zone of slope change in the behaviour of entropy when the cycle is classically evaluated. Additionally, we evaluate the total work and efficiency for classical and quantum Otto cycle, always finding, in the explored zones, that the work and efficiency for the classical cycle are larger than their quantum counterpart.

Acknowledgments: F. J. P. acknowledges the financial support of FONDECYT-postdoctoral 3170010, and D. Z. acknowledges to USM-DGIIP. P. Vargas acknowledge support from Financiamiento Basal para Centros Científicos y Tecnológicos de Excelencia, under Project No. FB 0807 (Chile), authors acknowledge to DTI-USM for the use of "Mathematica Online Unlimited Site" at the Universidad Técnica Federico Santa María

Author Contributions: F. J. P. , G. A. and P. V. conceived the idea and formulated the theory. O. N., D. Z and A .G. built the computer program and edited figures. A. S. N. and P. A. O. contributed to discussions during the entire work and the corresponding editing of the same. F. J. P. wrote the paper. All authors have read and approved the final manuscript.

Conflicts of Interest: The authors declare no conflict of interest.

References

1. Scovil, H.E.D.; Schulz-DuBois, D.O. Three-Level masers as a heat engines. *Phys. Rev. Lett.* **1959**, *2*, 262-263.
2. Feldmann, T.; Geva, E.; Kosloff, R. and Salamon, P. Heat engines in finite time governed by master equations. *American Journal of Physics* **1996**, *64*, 485.
3. Feldmann, T. and Kosloff, R. Characteristics of the limit cycle of a reciprocating quantum heat engine. *Phys. Rev. E* **2004** , *70*, 046110.
4. Rezek, Y. and Kosloff, R. Irreversible performance of a quantum harmonic heat engine. *New Journal of Physics* **2006**, *8*, 83.
5. Henrich, M. J.; Rempp, F. and Mahler, G. Quantum thermodynamic Otto machines: A spin-system approach. *The European Physical Journal Special Topics* **2007**, *151*, 157.
6. Quan, H. T.; Liu, Y. -x.; Sun, C. P., and Nori, F. Quantum thermodynamic cycles and quantum heat engines. *Phys. Rev. E* **2007**, *76*, 031105. 031105 (2007).
7. He, J.; He, X. and Tang, W. The performance characteristics of an irreversible quantum Otto harmonic refrigeration cycle. *Science in China Series G: Physics, Mechanics and Astronomy* **2009**, *52*, 1317.
8. Liu, S.; Ou, C. Maximum Power Output of Quantum Heat Engine with Energy Bath. *Entropy* **2016**, *18*, 205.
9. Scully, M.O.; Zubairy, M.S.; Agarwal, G.S.; Walther, H. Extracting work from a single heath bath via vanishing quantum coherence. *Science* **2003**, *299*, 862–864.
10. Scully, M.O.; Zubairy, M.S.; Dorfmann, K.E.; Kim, M.B.; Svidzinsky, A. Quantum heat engine power can be increased by noise-induced coherence. *Proc. Natl. Acad. Sci. USA* **2011**, *108*, 15097–15100.
11. Bender, C.M.; Brody, D.C.; Meister, B.K. Quantum mechanical Carnot engine. *J. Phys. A Math. Gen.* **2000**, *33*, 4427.
12. Bender, C.M.; Brody, D.C.; Meister, B.K. Entropy and temperature of quantum Carnot engine. *Proc. R. Soc. Lond. A* **2002**, *458*, 1519.
13. Wang, J.H.; Wu, Z.Q.; He, J. Quantum Otto engine of a two-level atom with single-mode fields. *Phys. Rev. E* **2012**, *85*, 041148.
14. Huang, X.L.; Xu, H.; Niu, X.Y.; Fu, Y.D. A special entangled quantum heat engine based on the two-qubit Heisenberg XX model. *Phys. Scr.* **2013**, *88*, 065008.
15. Muñoz, E.; Peña, F.J. Quantum heat engine in the relativistic limit: The case of Dirac particle. *Phys. Rev. E* **2012**, *86*, 061108.
16. Quan, H.T. Quantum thermodynamic cycles and quantum heat engines (II). *Phys. Rev. E* **2009**, *79*, 041129.
17. Zheng, Y.; Polleti, D. Work and efficiency of quantum Otto cycles in power-law trapping potentials. *Phys. Rev. E* **2014**, *90*, 012145.
18. Cui, Y.Y.; Chem, X.; Muga, J.G. Transient Particle Energies in Shortcuts to Adiabatic Expansions of Harmonic Traps. *J. Phys. Chem. A* **2016**, *120*, 2962.
19. Beau, M.; Jaramillo, J.; del Campo, A. Scaling-up Quantum Heat Engines Efficiently via Shortcuts to Adiabaticity. *Entropy* **2016**, *18*, 168.

20. Deng, J.; Wang, Q.; Liu, Z.; Hänggi, P.; Gong, J. Boosting work characteristics and overall heat-engine performance via shortcuts to adibaticity: Quantum and classical systems. *Phys. Rev. E* **2013**, *88*, 062122.
21. Wang, J.; He, J.; He, X. Performance analysis of a two-state quantum heat engine working with a single-mode radiation field in a cavity. *Phys. Rev. E* **2011**, *84*, 041127.
22. Abe, S. Maximum-power quantum-mechanical Carnot engine. *Phys. Rev. E* **2011**, *83*, 041117.
23. Wang, J.H.; He, J.Z. Optimization on a three-level heat engine working with two noninteracting fermions in a one-dimensional box trap. *J. App. Phys.* **2012**, *111*, 043505.
24. Wang, R.; Wang, J.; He, J.; Ma, Y. Performance of a multilevel quantum heat engine of an ideal N-particle Fermi system. *Phys. Rev. E* **2012**, *86*, 021133.
25. Jaramillo, J.; Beau, M.; del Campo, A. Quantum supremacy of many-particle thermal machines. *New J. Phys.* **2016**, *18*, 075019.
26. del Campo, A.; Goold, J.; Paternostro, M. More bang for your buck: Super-adiabatic quantum engines. *Sci. Rep. 4* **2017**, 14391.
27. Huang, X.L.; Niu, X.Y.; Xiu, X.M.; Yi, X.X. Quantum Stirling heat engine and refrigerator with single and coupled spin systems. *Eur. Phys. J. D* **2014**, *68*, 32.
28. Su, S.H.; Luo, X.Q.; Chen, J.C.; Sun, C.P. Angle-dependent quantum Otto heat engine based on coherent dipole-dipole coupling. *EPL* **2016**, *115*, 30002.
29. Kosloff, R.; Rezek, Y. The Quantum Harmonic Otto Cycle. *Entropy* **2017**, *19*, 136.
30. Roßnagel, J.; Dawkins, T.K.; Tolazzi, N.K.; Abah, O.; Lutz, E.; Kaler-Schmidt, F.; Singer, K. A single-atom heat engine. *Science* **2016**, *352*, 325.
31. Dong, C.D.; Lefkidis, G.; Hübner, W. Quantum Isobaric Process in Ni_2. *J. Supercond. Nov. Magn.* **2013**, *26*, 1589–1594.
32. Dong, C.D.; Lefkidis, G.; Hübner, W. Magnetic quantum diesel in Ni_2. *Phys. Rev. B* **2013**, *88*, 214421.
33. Hübner, W.; Lefkidis, G; Dong, C.D.; Chaudhuri, D. Spin-dependent Otto quantum heat engine based on a molecular substance. *Phys. Rev. B* **2014**, *90*, 024401.
34. Mehta, V.; Johal, R.S. Quantum Otto engine with exchange coupling in the presence of level degeneracy. *Phys. Rev. E* **2017**, *96*, 032110.
35. Azimi, M.; Chorotorlisvili, L.; Mishra, S.K.; Vekua, T.; Hübner, W.; Berakdar, J. Quantum Otto heat engine based on a multiferroic chain working substance. *New J. Phys.* **2014**, *16*, 063018.
36. Chotorlishvili, L.; Azimi, M.; Stagraczyński, S.; Toklikishvili, Z.; Schüler, M.; Berakdar, J. Superadiabatic quantum heat engine with a multiferroic working medium. *Phys. Rev. E* **2016**, *94*, 032116.
37. Muñoz, E.; Peña, F.J. Magnetically driven quantum heat engine. *Phys. Rev. E* **2014**, *89*, 052107.
38. Mani, R.G.; Smet, J.H.; von Klitzing, K.; Narayanamurti, V.; Johnson, W.B.; Umansky, V. Zero-resistance states induced by electromagnetic-wave excitation in GaAs/AlGaAs heterostructures. *Nature* **2002**, 420, 646–650.
39. Jacak, L.; Hawrylak, P. and Wójs, *Quantum Dots*, Springer-Verlag, 1998.
40. Muñoz, E.; Barticevic, Z. and Pacheco, M. Electronic spectrum of a two-dimensional quantum dot array in the presence of electric and magnetic fields in the Hall configuration. *Phys. Rev. B* **2005** *71*, 165301.
41. Quan, H.T.; Zhang, P.; Sun, C.P. Quantum heat engine with multilevel quantum systems. *Phys. Rev. E* **2005**, *72*, 056110.
42. Peña, F.J.; Muñoz, E. Magnetostrain-driven quantum heat engine on a graphene flake. *Phys. Rev. E* **2015**, *91*, 052152.
43. Wolfram Research, Inc., Mathematica, Version 11.3, Champaign, IL (2018).
44. Muñoz, E.; Peña, F.J.; González, A. Magnetically-Driven Quantum Heat Engines: The Quasi-Static Limit of Their Efficiency. *Entropy* **2016**, *18*, 173.
45. Callen, H. B. *Thermodynamics and an introduction to thermostatistics*, John Wiley & sons 1985.
46. Kumar, J.; Sreeram P. A. and Dattagupta, S., Low-temperature thermodynamics in the context of dissipative diamagnetism. *Phys. Rev. E* **2009**, *79*, 021130.